ORIGINAL ARTICLE

Molecular and Metabolic Evidence for Mitochondrial Defects Associated With β-Cell Dysfunction in a Mouse Model of Type 2 Diabetes

Hongfang Lu, Vasilij Koshkin, Emma M. Allister, Armen V. Gyulkhandanyan, and Michael B. Wheeler

OBJECTIVE—The inability of pancreatic β-cells to appropriately respond to glucose and secrete insulin are primary defects associated with β-cell failure in type 2 diabetes. Mitochondrial dysfunction has been implicated as a key factor in the development of type 2 diabetes; however, a link between mitochondrial dysfunction and defective insulin secretion is unclear.

RESEARCH DESIGN AND METHODS—We investigated the changes in islet mitochondrial function and morphology during progression from insulin resistance (3 weeks old), immediately before hyperglycemia (5 weeks old), and after diabetes onset (10 weeks old) in transgenic MKR mice compared with controls. The molecular and protein changes at 10 weeks were determined using microarray and iTRAQ proteomic screens.

RESULTS—At 3 weeks, MKR mice were hyperinsulinemic but normoglycemic and β-cells showed negligible mitochondrial or morphological changes. At 5 weeks, MKR islets displayed abrogated hyperpolarization of mitochondrial membrane potential ($\Delta\Psi_m$), reduced mitochondrial Ca^{2+} uptake, slightly enlarged mitochondria, and reduced glucose-stimulated insulin secretion. By 10 weeks, MKR mice were hyperglycemic and hyperinsulinemic and β-cells contained swollen mitochondria with disordered cristae. β-Cells displayed impaired stimulus-secretion coupling including reduced hyperpolarization of $\Delta\Psi_m$, impaired Ca^{2+}-signaling, and reduced glucose-stimulated ATP/ADP and insulin release. Furthermore, decreased cytochrome c oxidase–dependent oxygen consumption and signs of oxidative stress were observed in diabetic islets. Protein profiling of diabetic islets revealed that 36 mitochondrial proteins were differentially expressed, including inner membrane proteins of the electron transport chain.

CONCLUSIONS—We provide novel evidence for a critical role of defective mitochondrial oxidative phosphorylation and morphology in the pathology of insulin resistance–induced β-cell failure. *Diabetes* 59:448–459, 2010

Insulin resistance is the earliest detectable abnormality in patients at high risk of developing type 2 diabetes (1); however, recurring findings from clinical studies reveal that insulin resistance alone is insufficient to cause diabetes. Patients in early-stage type 2 diabetes always present with defects in pancreatic β-cell insulin secretion (2,3); however, the mechanisms involved in β-cell failure are largely unknown.

Pancreatic β-cells sense changes in blood glucose and secrete insulin to maintain normoglycemia. Glucose sensing in β-cells is largely controlled by the activity of glucokinase (4) and mitochondrial metabolism, which drives the respiratory chain and subsequently ATP production via oxidative phosphorylation (OxPhos). The critical regulatory role of ATP production by OxPhos is underscored by the observation that disrupting mitochondrial oxidative metabolism blocks glucose-stimulated insulin secretion (GSIS) (5,6). After closure of the ATP-sensitive K^+ (K_{ATP}) channels, Ca^{2+} enters the cytosol and triggers the secretion of insulin from the cell. Thus, in response to changes in nutrient supply, there is a complementary regulation of OxPhos and other mitochondrial factors to maintain cellular ATP and NADH levels, providing efficient metabolic coupling signals to trigger insulin secretion.

A pivotal role of mitochondria in the pathogenesis of type 2 diabetes is underlined by the finding that mitochondrial DNA (mtDNA) mutations in humans, as well as pancreatic β-cell–specific deletion of mitochondrial genes in animal models, reduces OxPhos capacity and causes diabetes (7,8). Recent data suggest that β-cells normally contain a filamentous network of mitochondria, but when mitochondria become chronically fused or fragmented, GSIS is impaired (9–11). Abnormal mitochondrial morphology and function was observed in pancreatic β-cells postmortem from type 2 diabetic patients (12,13). However, there is currently no information on how mitochondria in human β-cells adapt when an individual becomes insulin resistant (14). Several studies have implicated impaired skeletal muscle mitochondrial OxPhos, increased oxidative stress, and altered morphology in the etiology of insulin resistance, proposing a mechanism for the development of diabetes and obesity (15–17). It is possible that similar changes occur in β-cells and so to understand whether β-cell mitochondrial dysfunction is causative or correlative in the process of insulin resistance leading to hyperglycemia/β-cell dysfunction, we have studied the transgenic MKR mouse (18). One unique feature of the MKR mouse is that it does not harbor a β-cell genetic defect, but rather a dominant-negative IGF-I receptor mutation specifically in skeletal muscle. This causes muscle insulin resistance early in life followed by systemic

insulin resistance and finally β-cell dysfunction and hyper-glycemia by 8 weeks of age (18,19). In contrast with other insulin-resistant models, MKR mice allow the study of progression from insulin resistance to type 2 diabetes in the absence of obesity (20).

In this study, we systematically characterized and compared mitochondrial morphology, metabolic function, and the molecular changes at three time points in *1*) insulin resistance (3 weeks old), *2*) glucose intolerant but just before the onset of hyperglycemia (5 weeks old), and *3*) diabetic (10 weeks old) MKR mouse islets. Our study provides the following findings: *1*) insulin resistance alone is not associated with pancreatic β-cell mitochondrial dysfunction; *2*) decreased mitochondrial function and abnormal morphology occurs before the onset of hyper-glycemia and plays a role in β-cell failure and type 2 diabetes in MKR mice; *3*) proteins in the mitochondrial inner membrane, including rate-limiting enzymes of the TCA cycle and multiple components involved in OxPhos, are decreased in MKR diabetic islets; and *4*) genomic and proteomic analyses reveal transcriptional changes of a subset of mitochondrial proteins that account for changes in protein abundance; however, translational and post-translational modifications also influence the expression of other mitochondrial proteins in diabetic β-cells. There-fore, defective mitochondrial OxPhos and morphology play a critical role in the pathology of insulin resistance–induced β-cell dysfunction.

RESEARCH DESIGN AND METHODS

Reagents. Fluorescent dyes Rhod-2 and Rh123 were from Molecular Probes (Eugene, Oregon). Dispase II was from Roche Diagnostics (Germany). Other reagents were from Sigma-Aldrich Canada.

Animal care. Mice were maintained in a 12-h light/dark cycle and had free access to water and food (diet no. 8664; Harlan Tekland, Madison, WI). MKR and FVB male mice were used as described previously (19). Animal care was conducted according to protocols and standards of the Canadian Council on Animal Care and approved by the Animal Care and Use Committee at the University of Toronto.

Mouse pancreatic islet isolation and dispersion. Pancreatic islets were isolated as described previously (21).

Ultrastructural islet analysis. Electron microscopic analysis was completed on islets isolated from five to seven mice per genotype essentially as previously described (22). The samples were observed under a Philips CM100 electron microscope operating at 75 kV. Images were recorded digitally using a Kodak 1.6 Megaplus camera system operated using AMT software (Advanced Microscopy Techniques Corporation). β-Cells were recognized by the typical ultrastructural appearance (13). The area and number of β-cell mitochondrion and dense core insulin granules were quantified by analyzing 50–100 10,000× magnification electron microscopic images from random areas of islets isolated from each mouse. Area and number were determined by using the threshold setting and the particle analysis tool in Image J software.

Islet GSIS and ATP/ADP ratio. Islet insulin secretion and ATP/ADP measurements were performed as described previously (23). Total islet ATP/ADP ratio was determined in the islets after GSIS using the ApoSENSOR ATP/ADP Ratio Assay Kit (BioVision, Mountain View, CA).

Mitochondrial membrane potential. Mitochondrial membrane potential ($\Delta\Psi_m$) was measured using Rh123 in dispersed β-cells as reported previously (21). Fluorescent responses after the addition of nutrient substrates (11 mmol/l glucose or 10 mmol/l ketoisocaproic acid [KIC]) and the respiration inhibitor (5 mmol/l sodium azide) were compared with baseline (1 mmol/l glucose) and used to characterize mitochondrial hyperpolarization and depo-larization, respectively. A decrease in fluorescence corresponded to an increase in $\Delta\Psi_m$. The identification of β-cells was based on size and mitochondrial hyperpolarization (21).

Mitochondrial Ca^{2+} imaging. Dispersed islet cells were loaded with Rhod-2 (1 μmol/l) during a 45-min pretreatment at 37°C in Krebs-Ringer buffer. The loaded cells were transferred to a perifusion chamber on the thermo platform of an Olympus fluorescent BX51W1 microscope. Images were collected using 540 nm excitation and tetramethylrhodamine methyl ester emission filter set.

Estimation of oxidation of 2′,7′-dichlorodihydro-fluorescein-diacetate (DCF). Oxidative stress was estimated in dispersed β-cells using the fluorescence emission of 2′,7′-dichlorodihydro-fluorescein-diacetate (DCF) as reported previously (24).

Respiration measurements. O$_2$ consumption was measured using a Clark-type electrode coupled to an Oxygraph unit (Hansatech, Pentney, U.K.). Freshly isolated, dispersed, and permeabilized (with saponin, 80 μg/ml, 5 min) islets were suspended at a concentration of 0.6–0.9 mg protein/ml in incubation medium containing 0.25 mol/l sucrose, 10 mmol/l HEPES, 1 mmol/l MgCl$_2$, 20 μmol/l EGTA, and 0.1% BSA, pH 7.3. Ascorbic acid (10 mmol/l) and N,N,N′,N′-tetramethyl-*p*-phenylenediamine (TMPD) (0.4 mmol/l) were added as substrate and used to estimate cytochrome c oxidase activity (25). Oxygen kinetic traces were analyzed by measuring the slopes of the oxygen consumption curves minus background. Respiration rates were converted into molar oxygen units using O$_2$ solubility in sucrose medium, as previously reported (21).

RNA extraction, gene expression profile, and quantitative RT-PCR. Sample processing, microarray experiments, and quantitative PCR were performed as described previously (26), and primers are listed in supplemental Table S4 in the online appendix available at http://diabetes. diabetesjournals.org/cgi/content/full/db09-0129/DC1.

Mitochondrial DNA analysis. Total DNA was extracted from islets using a QIAamp DNA Mini Kit (Qiagen, Germany). The content of mtDNA was calculated using quantitative PCR by measuring the ratio of mitochondrially encoded *Cox1*, *Cox2*, and *Cox3* versus a nuclear-encoded gene (β-*actin*).

Proteomic analysis. The global protein expression profiles of freshly isolated islets from 10-week-old MKR and control mice were determined using the isobaric tags for relative and absolute quantification (iTRAQ) quantitative proteomic approach combined with high-performance liquid chromatography mass spectrometry/mass spectrometry (HPLC-MS/MS). Three independent iTRAQ analyses using islets from 8–10 mice were performed. The detailed experimental design and results were reported elsewhere (26). Cluster analysis of detected mitochondrial proteins was performed using GoMiner (27) and GeneMAPP (28) programs.

Statistical analysis. All experiments were performed with islets pooled from at least three to five mice of each genotype and three to six independent preparations. Results are expressed as means ± SE. Statistical significance was assessed using either a Student's *t* test or one-way or two-way ANOVA for repeated measures followed by multiple Bonferroni comparisons. *P* < 0.05 was considered statistically significant.

RESULTS

Insulin secretion and ATP/ADP ratio. At 3 weeks of age, MKR mice are normoglycemic, but have significantly increased fasting plasma insulin levels (*P* < 0.001) compared with WT (Fig. 1*A* and *B*). Five weeks of age represents the time point just before the onset of hyper-glycemia in MKR mice, whereas at 6 weeks, their blood glucose is ~20 mmol/l (19). In contrast, 10-week-old MKR mice were clearly hyperglycemic (*P* < 0.001) and hyper-insulinemic (*P* < 0.001), and this was consistent with previous results (Fig. 1*A* and *B*) (18,26). MKR mice are hyperlipidemic by 3 weeks of age, and their plasma triglycerides remain elevated throughout their lifespan (18,29). Ex vivo islet characterization revealed no significant difference in GSIS or ATP/ADP ratio at 3 weeks of age (Fig. 1*C* and *E*). Islets isolated from 5- and 10-week-old MKR mice had significantly higher basal insulin secretion (data not shown) but did not stimulate secretion to the same extent as WT islets in the presence of high glucose (Fig. S1 in the online appendix and Fig. 1*D*). Islets from 10-week-old WT mice showed increased total intracellular ATP/ADP ratio after glucose stimulation, whereas islets from diabetic MKR mice showed a blunted response (Fig. 1*F*).

Mitochondrial membrane potential. Oxidative phos-phorylation produces a proton gradient across the inner mitochondrial membrane, which hyperpolarizes the mito-chondrial membrane and drives ATP synthesis. Therefore, we measured changes in $\Delta\Psi_m$ in β-cells using Rhodamine 123 (Rh123) under nutrient stimulation (30). At all ages,
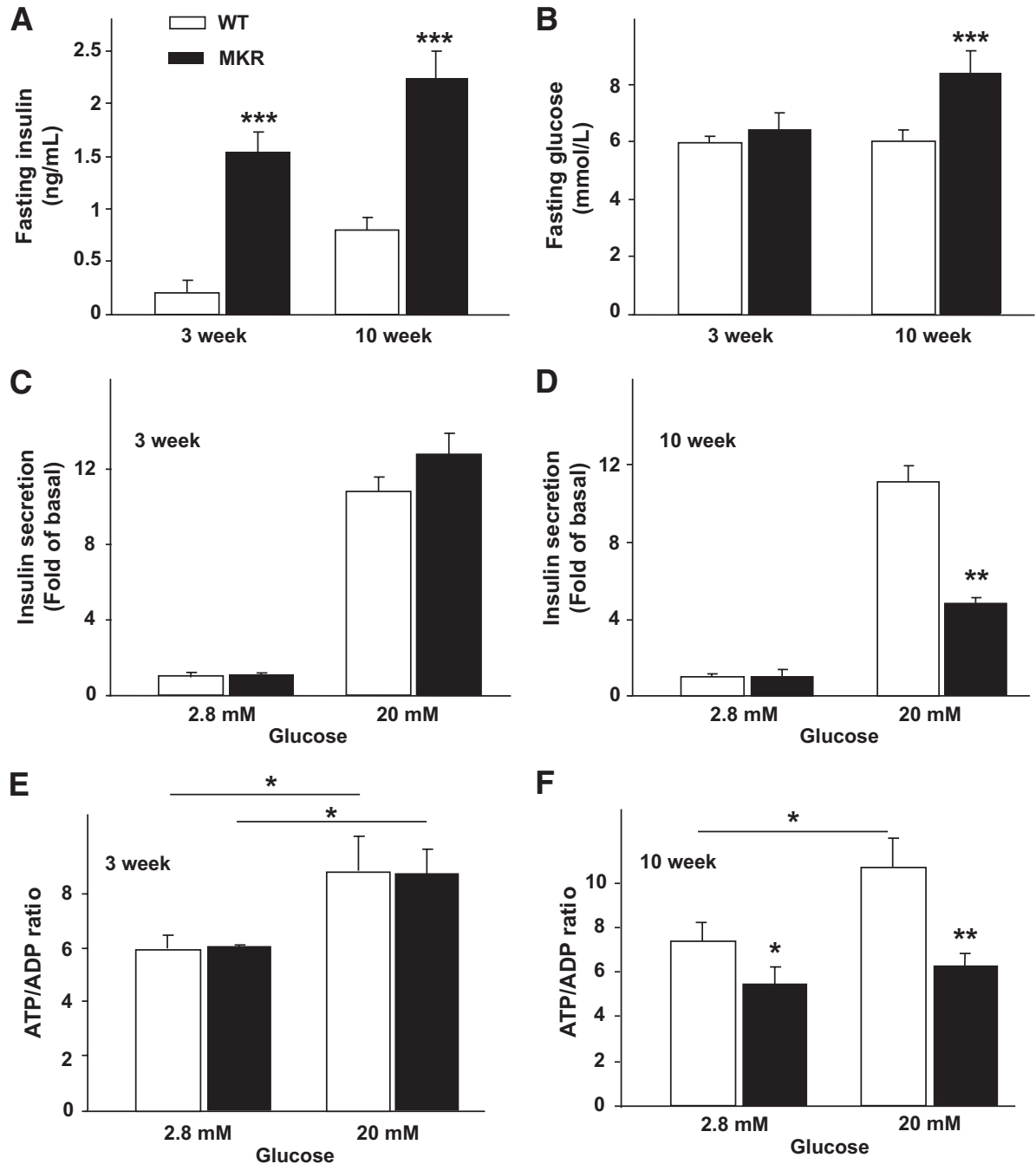
FIG. 1. Mouse characterization and islet glucose-stimulated insulin secretion and ATP/ADP ratio. Fasting plasma insulin (*A*) and blood glucose levels (*B*). Islets from age-matched MKR and WT mice were exposed to 2.8 or 20 mmol/l glucose. *C* and *D*: Islet insulin secretion during 1 h in 3- and 10-week-old islets. GSIS from 5-week-old islets is shown in Fig. S1. *E* and *F*: Total islet ATP/ADP ratio. (*n* = 3 independent experiments with five mice per genotype.) Data are means ± SE. *$P < 0.05$; **$P < 0.01$; ***$P < 0.001$ MKR compared with age-matched WT unless otherwise indicated.

the addition of 11 mmol/l glucose hyperpolarized (decreased Rh123 fluorescence) and 5 mmol/l of the respiratory inhibitor NaN_3 completely depolarized $\Delta\Psi_m$ (Fig. 2*A–C* and Fig. S2*A* in the online appendix). There was no difference in glucose-induced hyperpolarization of $\Delta\Psi_m$ in β-cells from 3-week-old MKR and control mice. However, β-cells from 5- and 10-week-old MKR mice showed a 46 and 41% decrease in hyperpolarization of $\Delta\Psi_m$, respectively, suggesting defective glucose metabolism and mitochondrial function (Fig. 2*C*). Defective mitochondrial function was further substantiated using KIC, which is a direct substrate for the mitochondrial TCA cycle and

bypasses glycolysis (31). β-Cells from 3-week-old MKR and control mice (Fig. 2*D* and *F*) exhibited a similar response to KIC, whereas β-cells from 5- and 10-week-old MKR mice displayed 41 and 56% lower hyperpolarization of $\Delta\Psi_m$, respectively (Fig. 2*E* and *F* and Fig. S2*B* in the online appendix).

Mitochondrial Ca^{2+}. The uptake of Ca^{2+} into the mitochondria reflects mitochondrial metabolic capacity and potentially activates key dehydrogenases of the TCA cycle and OxPhos (32). At 3 weeks of age, 11 mmol/l glucose caused a similar increase in Rhod2 fluorescence in islets from MKR and WT mice (Fig. 3*A* and *B*), indicating similar
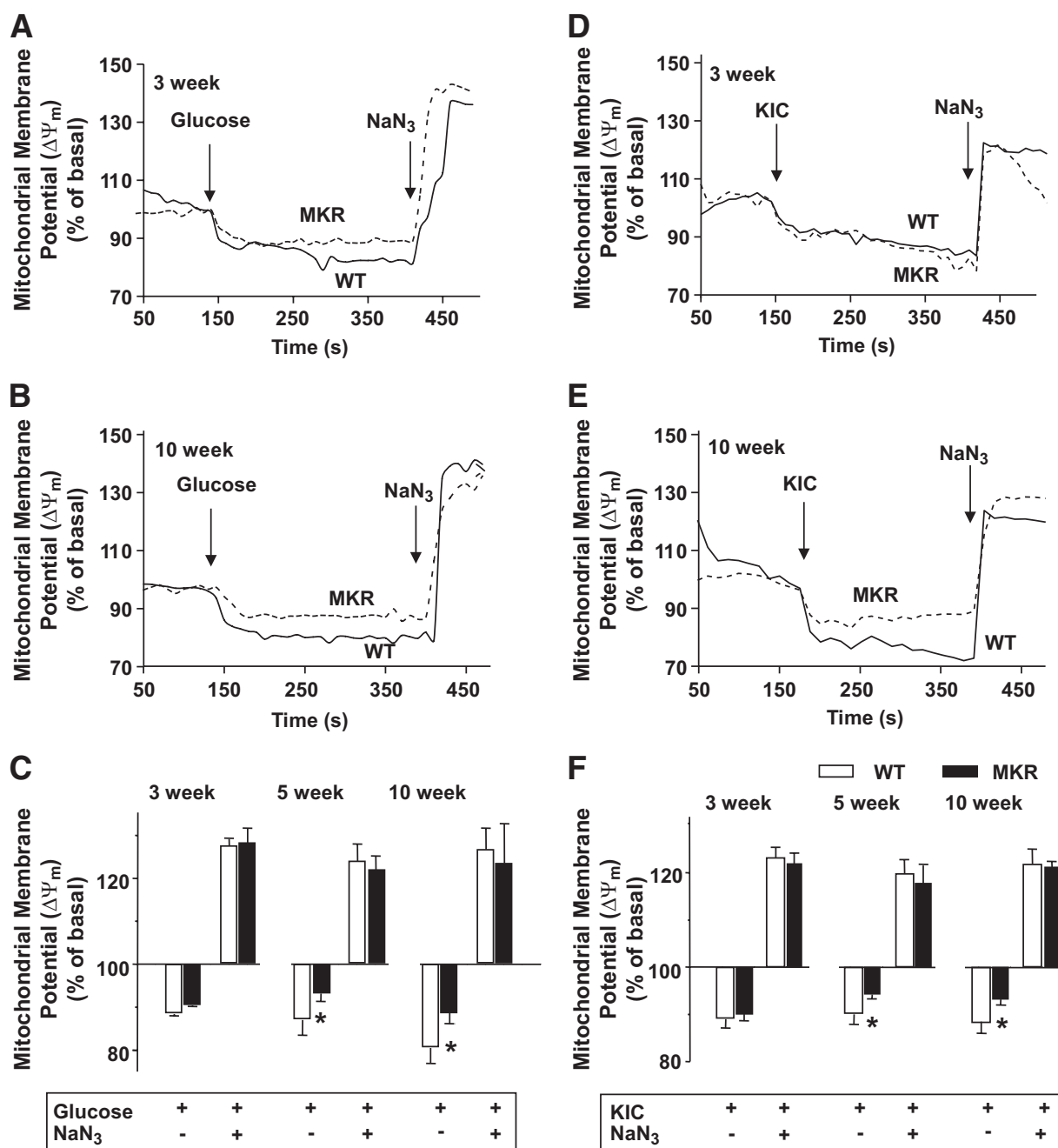
FIG. 2. Decreased mitochondrial membrane potential ($\Delta\Psi_m$) in 5- and 10-week-old MKR β-cells. Mitochondrial membrane potential was measured using Rh123 in dispersed islet cells from 3-week-old (*A* and *D*), 5-week-old (Fig. S2), and 10-week-old (*B* and *E*) MKR (gray dashed lines) and WT (solid black lines) mice. Mitochondrial membrane potential was estimated by the difference in Rh123 fluorescent signals between hyperpolarized (glucose, 11 mmol/l, *A* and *B*; ketoisocaproate [KIC], 10 mmol/l, *D* and *E*) and basal and fully depolarized (sodium azide, 5 mmol/l) states. *A*, *B*, *D*, and *E*: Representative kinetic traces of the fluorescent signal from a single β-cell. *C* and *F*: Summary of $\Delta\Psi_m$ changes compared with basal levels in WT (□) and MKR (■) islet cells. Results are the percent change from basal fluorescence (1 mmol/l glucose before additions) (*n* = 3–5 independent experiments, and each experiment used 30–50 cells from three mice per genotype). Data are means ± SE. *$P < 0.05$ compared with age-matched WT.

mitochondrial calcium $[Ca^{2+}]_m$ accumulation. However, islets from 5-week-old mice showed a significant 40% reduction ($P < 0.05$) (Fig. 3*C* and *D*) and 10-week-old diabetic islets showed an even greater 60% attenuation in $[Ca^{2+}]_m$ uptake in response to high glucose stimulation, compared with WT ($P < 0.001$) (Fig. 3*E* and *F*). Direct confirmation of reduced $[Ca^{2+}]_m$ loading capacity in MKR islets was obtained using permeabilized β-cells (Fig. S3) and a slight but significant reduction in cytosolic Ca^{2+} uptake was observed in whole islets from 6- and 10-week-old MKR mice ($P < 0.05$) (Fig. S4).

Mitochondrial respiration. Maximal respiratory capacity of islet mitochondria was estimated by measuring the activity of complex IV (cytochrome c oxidase) while using ascorbic acid as substrate (25). The rate of decrease in oxygen tension in the chamber, reflecting respiration by mitochondria, was significantly lower in 10-week-old MKR diabetic islet cells compared with WT ($P < 0.01$), indicating reduced mitochondrial oxidative capacity (Fig. 3*G* and *H*).

Mitochondrial morphology. We documented mitochondrial morphology changes in pancreatic β-cells of hyper-
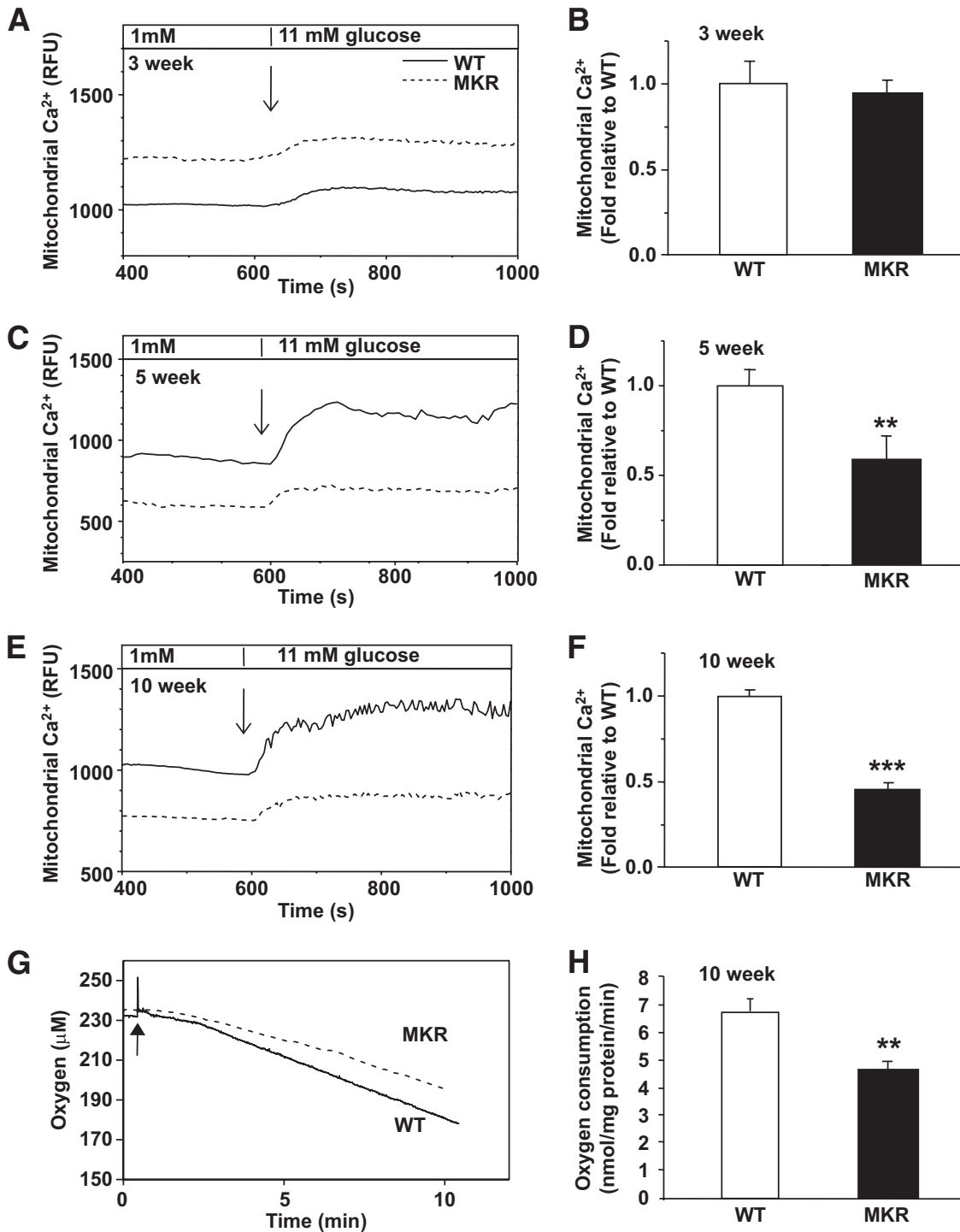
FIG. 3. Reduced mitochondrial Ca^{2+} accumulation and respiration in MKR islets. Islets from 3-week-old (*A*), 5-week-old (*C*), and 10-week-old (*E*) mice were loaded with Rhod-2 and photon emission monitored in a chamber perifused with Krebs-Ringer buffer containing basal (1 mmol/l) and 11 mmol/l glucose. *A*, *C*, and *E*: Representative kinetic traces from a single islet are shown and families of traces from three to four islets per genotype are shown in Fig. S5. *B*, *D*, and *F*: Summary of the difference in Rhod-2 fluorescence (relative fluorescent units [RFU]) between basal (1 mmol/l) and maximal (11 mmol/l) glucose (*n* = 3–5 independent experiments, and each experiment contains nine islets from three mice per genotype). *G* and *H*: O_2 consumption in 10-week-old islets supported by respiratory substrates for complex IV (ascorbate and TMPD) was measured. Addition of ascorbate/TMPD (10 mmol/l/0.4 mmol/l) is marked by an arrow. *G*: Representative trace. *H*: The slopes of the oxygen consumption curves were measured between 5 and 10 min, the background ascorbate/TMPD effect in the absence of islets was subtracted, and genotypes were compared. WT = solid black line; MKR = gray dotted line (*n* = 3 with 8–10 mice per genotype in each experiment). Data are means ± SE. **$P < 0.01$; ***$P < 0.001$ compared with age-matched WT.

insulinemic (3 weeks old), just before hyperglycemia (5 weeks old), and diabetic (10 weeks old) MKR mice using electron microscopy. β-Cells in 3-week-old MKR and WT mice had similar mitochondrial morphology (Fig. 4*A* and

B). Further quantitative analysis revealed no significant difference in mitochondrial number and area or insulin granule number (Fig. 4*C* and *J* and Fig. S6*A*–*C* in the online appendix). β-Cells from 5-week-old WT mice showed
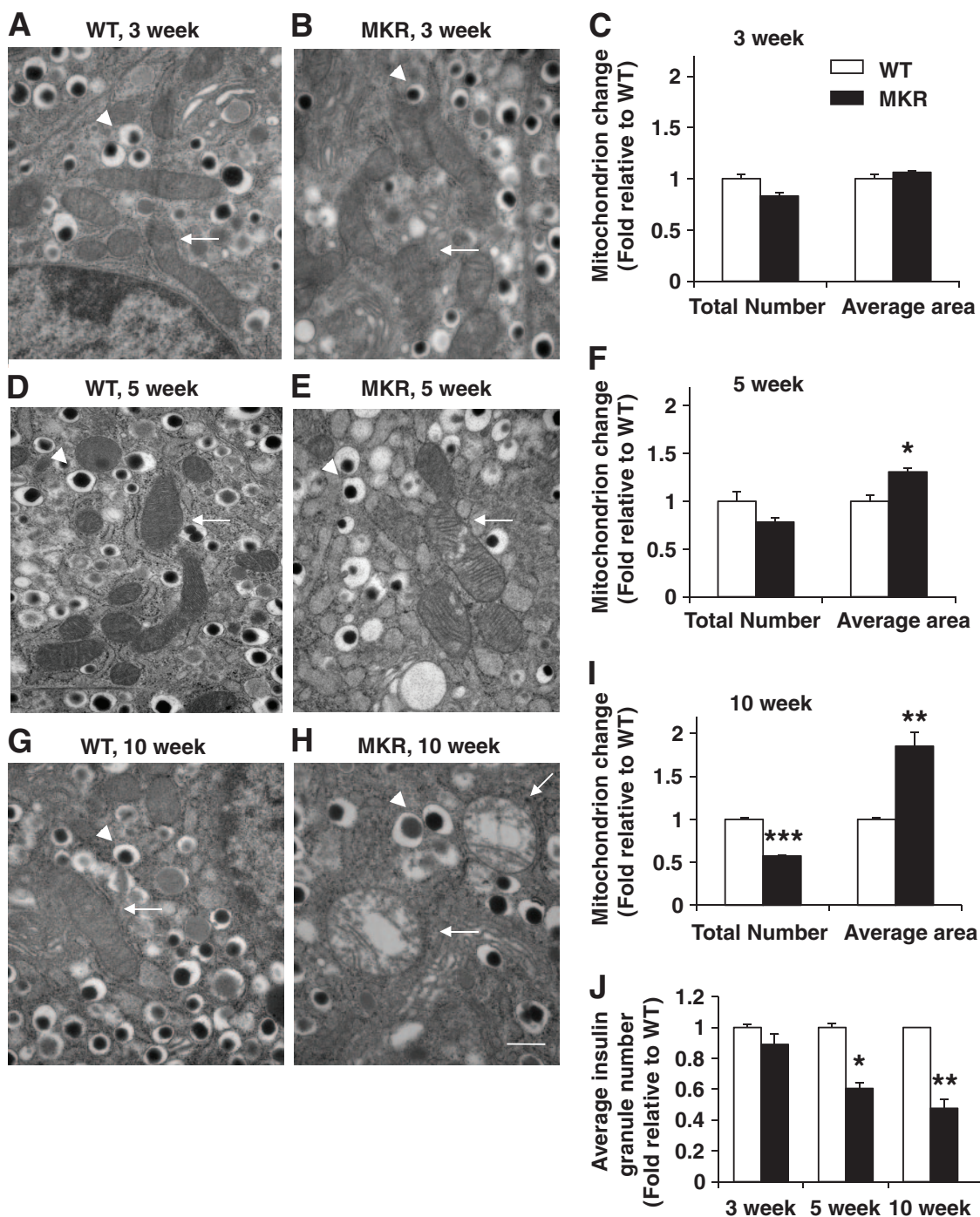
FIG. 4. Mitochondrial ultrastructure is disordered, and dense core insulin granule number is decreased in pancreatic β-cells from 5- and 10-week-old MKR islets. Electron micrographs are shown of ultra-thin sections of islets. β-Cells from 3-week-old WT mice (*A*) and MKR mice (*B*) had normal mitochondria (*C*). Mitochondria in β-cells of 5-week-old MKR mice (*E*) were slightly swollen (*F*). The mitochondria of β-cells from 10-week-old MKR diabetic mice (*H*) were reduced in number and severely swollen with disordered cristae (*I*) compared with normal mitochondrial morphology in WT control (*G*). 30,000× magnification. Scale bar equals 500 nm and is shown in the bottom right in *H*. White arrows indicate mitochondria. Arrowheads indicate insulin granules. Quantitation of total number of mitochondria and average mitochondrial area in 3-week-old (*C*), 5-week-old (*F*), and 10-week-old (*I*) WT and MKR electron microscopic sections. Dense core insulin granules were counted in images at 10,000× magnification (Fig. S6) and number was quantified (*J*). A total of 50–100 images were analyzed per age with 5–7 mice per genotype. Data are means ± SE. *$P < 0.05$; **$P < 0.01$; ***$P < 0.001$ compared with age-matched WT.

abundant insulin granules and mitochondria (Fig. 4*D* and Fig S6*D*), whereas MKR β-cells contained significantly less granules ($P < 0.05$) (Fig. 4*J* and Fig S6*E* and *F*), 22% fewer mitochondria ($P = 0.1$), and 30% larger mitochondria ($P < 0.05$) (Fig. 4*E* and *F*). By 10 weeks of age, MKR β-cells contained significantly less granules ($P < 0.001$) (Fig. 4*J* and Fig S6*G–I*) and 43% fewer mitochondria ($P < 0.001$); how-

ever, each mitochondria was ~75% larger ($P < 0.01$) (Fig. 4*H* and *I*) compared with WT. Notably, the mitochondria in these cells were often swollen, and the inner mitochondrial membranes had a disrupted structure with abnormal cristae.

Molecular defects in MKR diabetic islets

Genomics. To investigate the molecular defects responsible for the altered mitochondrial morphology and

metabolic coupling in MKR β-cells, we performed a simultaneous analysis of transcript and protein expression profiles in freshly isolated islets from 10-week-old MKR and WT mice (Table S1 and S2; Fig. 5 and Fig. S7). Using the GoMiner software (27), we determined that 55 of 854 differentially expressed genes were located in mitochondria based on Gene Ontology nomenclature. Approximately 50% (29 genes) of those genes were reduced in MKR diabetic islets. Cluster analysis revealed that 17 genes in the mitochondrial inner membrane were dysregulated in diabetic islets, with 65% of them being reduced. Several genes related to cell apoptosis, including *CYCS*, *LGALS12*, and *SGPP1*, were upregulated in MKR diabetic islets, whereas genes involved in glutamate metabolism were decreased (Fig. 5*D* and Fig. S7*D*). Genes in the OxPhos pathway, including *Atp5o*, *Atp5g1*, *Ndufa1*, and *Ndufa3*, were increased in MKR diabetic islets (Fig. 5*F*). Interestingly, neither the microarray nor qPCR results revealed a significant difference in the expression of transcription factors and co-regulators such as nuclear respiratory factor 1 (*NRF1*), *PGC1a*, *ESRRA*, *GABPA*, *GABPB*, *Tfam*, *Mfn2*, *Polg1*, and *Ucp2* between the two genotypes (Fig. S7*C*). These genes have previously been implicated in regulation of the mitochondrial electron transport chain and mitochondrial biogenesis (16,17).

Proteomics. Protein expression ultimately affects cellular function, so we performed global protein profiling of islets to complement the microarray data. Using an iTRAQ proteomic strategy combined with HPLC-MS/MS, ~590 unique proteins were detected at 95% confidence in islets from 10-week-old MKR and WT mice (26). Cluster analysis based on subcellular location revealed 107 proteins belonging to the mitochondrial compartment, and 36 of these proteins were differentially expressed in MKR diabetic islets versus control (Fig. 5*B*, Table S3). Remarkably, ~61% (22 proteins) of changed mitochondrial proteins were located in the inner mitochondrial membrane, and all but one (CYCS) of these proteins were decreased (Fig. 5*B* and Fig S8*B*). Those inner membrane proteins are mainly involved in mitochondrial OxPhos and include key enzymes in the TCA cycle, β-oxidation, glutamate metabolism, and electron transport chain (Fig. 5*B–F*). A comparison of the 55 differentially expressed genes and 36 proteins revealed only 10 gene-protein pairs that changed similarly at both the mRNA and protein level (Fig. 5*A* and *B*), implying that posttranslational modifications must contribute significantly to the decrease in protein and altered mitochondrial phenotype.

DCF fluorescence and mtDNA measurement. We quantified the amount of DCF fluorescence and measured the expression of antioxidant genes by qRT-PCR (24,33). At 3 weeks of age, MKR and WT dispersed islets showed similar oxidation of DCF and no major differences in antioxidant enzyme expression (Fig. 6*A*, *B*, and *E* and Fig. S9*A*). However, at 10 weeks of age, MKR islet cells exhibited a marked twofold increase in the fluorescent signal from oxidized DCF ($P < 0.001$) and significantly upregulated antioxidant gene expression compared with WT (Fig. 6*C*, *D*, and *F* and Fig. S9*B*). Chronic exposure to pro-oxidants leads to mtDNA damage in a variety of experimental models (16,34). The ratio of mtDNA to nuclear DNA in islets isolated from 3-week-old mice was similar (Fig. 6*G*); however, mtDNA content was significantly lower in 10-week-old MKR islets (Fig. 6*H*).

DISCUSSION

Our study reveals that mitochondrial defects do not appear during the early stages of insulin resistance (3-week-old MKR mice); however, just before the onset of hyperglycemia, mitochondrial defects are already apparent, and when the mice are diabetic (hyperglycemic, hyperinsulinemic, and hyperlipidemic [35]), there are clear metabolic and morphological defects in β-cell mitochondria. Consistent with abnormalities in mitochondrial morphology and decreased OxPhos, 22 of 36 differentially expressed mitochondrial proteins were located in the inner membrane, and 95% of them were decreased in MKR diabetic islets. Complexes I–IV of the electron transport chain are located at the inner mitochondrial membrane, and the flux of electrons along this respiratory chain establishes the proton gradient, which in turn generates the $\Delta\Psi_m$ and drives the production of ATP. In β-cells from MKR mice, just before and after the onset of hyperglycemia, glucose-induced hyperpolarization of $\Delta\Psi_m$ was reduced compared with control. Our finding is in agreement with a study that showed lower glucose-induced $\Delta\Psi_m$ and ATP/ADP ratio in islets from human type 2 diabetic patients (12). These changes could be mediated by reduced glucose sensing, reduced mitochondrial metabolism, or a combination of both. However, the reduced $\Delta\Psi_m$ hyperpolarization in response to KIC (which is a direct substrate for the TCA cycle, bypassing glycolysis) suggests that impaired glucose sensing is not the primary defect. No alteration in glucokinase expression (data not shown) corroborates this idea. Despite having significantly less insulin granules at 5 and 10 weeks of age, the MKR mice maintain the ability to secrete insulin in vivo in response to potent secretagogues such as arginine (19). Therefore, the inability of glucose to hyperpolarize $\Delta\Psi_m$ is likely a key defect, resulting in a reduced ATP/ADP ratio and GSIS.

The proteomic scan of MKR diabetic islets revealed decreased expression of multiple proteins involved in oxidative metabolism, including several components of the mitochondrial respiratory chain. The reduction of three components in complex IV, which regulates COX activity in response to ATP binding (36), may be responsible for the lower rate of cytochrome *c* oxidase–dependent oxygen consumption in MKR diabetic islets. Decreased cytochrome *c* oxidase activity has previously been demonstrated in islets from a diabetic patient (37), and a critical role of mitochondrial substrate oxidation in the β-cell has been demonstrated in patients with mutations in the mitochondrial genome (38). Similarly, we observed that proteins related to oxidative pathways were decreased in 10-week-old diabetic islets. Electron transfer flavoproteins are necessary electron acceptors for many dehydrogenases in the mitochondria, which then transfer electrons to the mitochondrial respiratory chain via electron transfer flavoprotein–ubiquinone oxidoreductase (39). The reduction in electron transfer flavoproteins likely reduces flux through the respiratory chain in MKR β-cells. Furthermore, downregulation of the adenine nucleotide translocator (SLC25A4) was observed in MKR islets. Adenine nucleotide translocators transfer ATP to the cytosol in exchange for ADP (40). Collectively, the downregulation of these numerous mitochondrial proteins in MKR islets are likely associated with the decreased oxidative function, ATP production and transport, and consequently impaired GSIS.
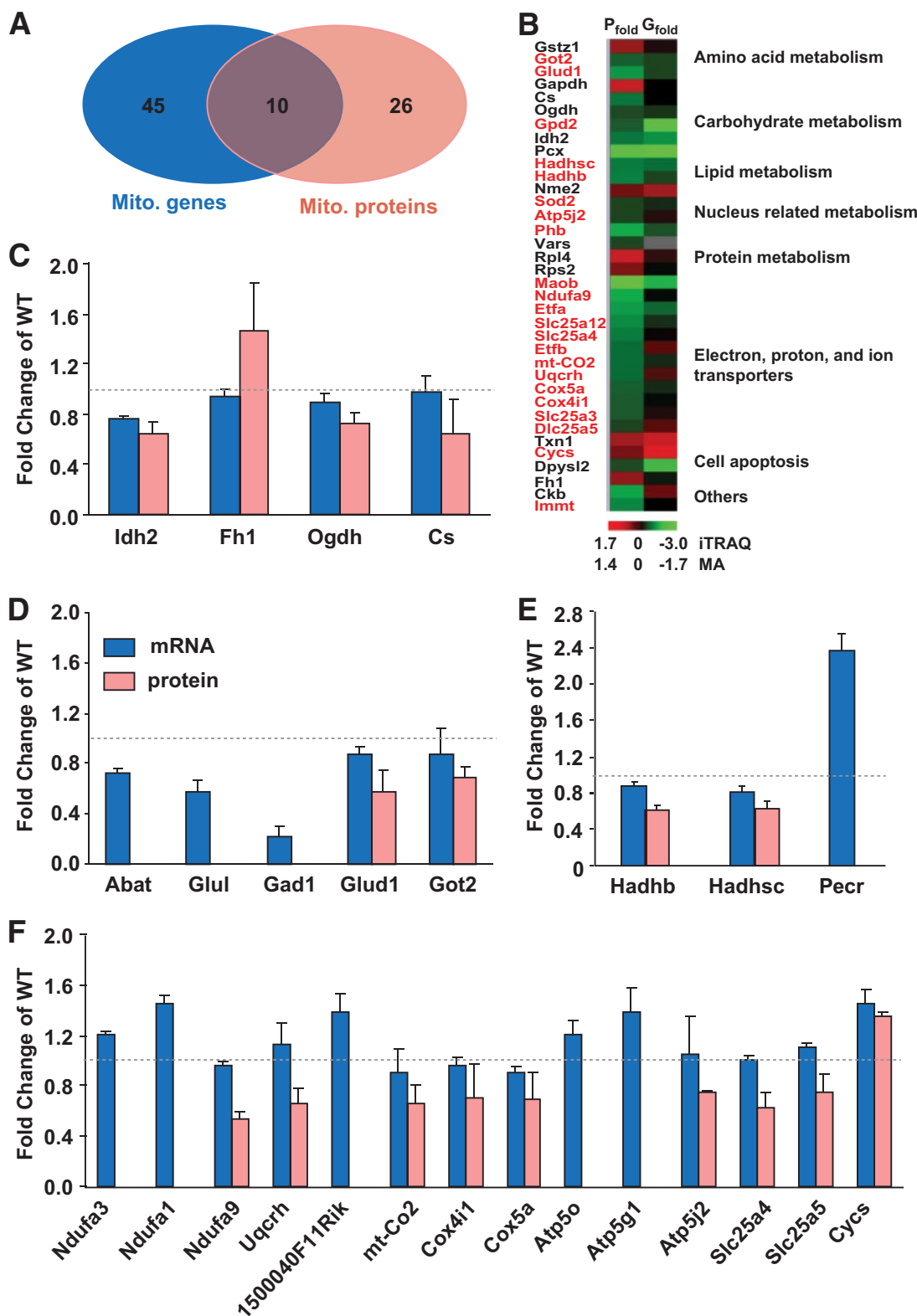
FIG. 5. Mitochondrial genes/protein changes in islets from 10-week-old mice. *A*: An integrated genomics and proteomics approach revealed 55 mitochondrial genes (Mito. gene) and 36 mitochondrial proteins (Mito. protein) that were significantly differentially expressed in 10-week-old MKR diabetic islets, 10 of which were changed at both the protein and mRNA level. *B*: A pictorial comparison of changed mitochondrial protein ratios (P_{fold}) detected by iTRAQ and microarray (MA) (G_{fold}) analysis together with functional cluster analysis. Hierarchical clustering was performed using the GoMiner program (27) based on the biological process category in the Gene Ontology Consortium. Colors represent average gene/protein expression changes (MKR/WT) relative to the median (26) with red and green representing an increase or decrease in fold expression, respectively. Red labels: mitochondrial inner membrane. *C–F*: Differentially expressed mitochondrial genes/proteins in MKR diabetic islets related to the TCA cycle (*C*), glutamate metabolism (*D*), fatty acid metabolism (*E*), and electron transport chains (*F*). Categorical analysis is based on KEGG pathway database using the GeneMAPP program (28). Data are means ± SE. All changes are significant ($P < 0.05$) compared with age-matched WT.
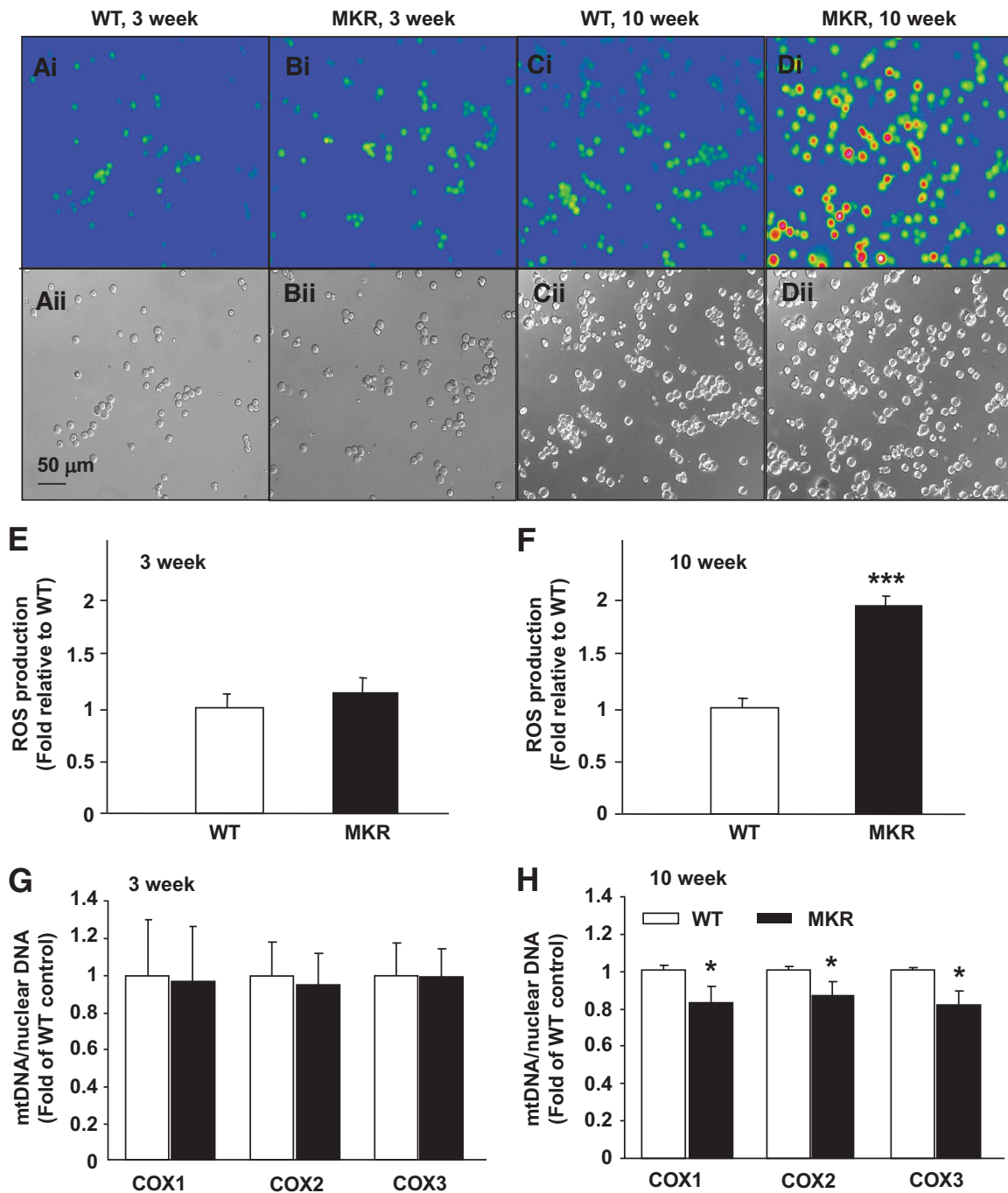
FIG. 6. Increased pro-oxidant levels and mitochondrial DNA damage in MKR diabetic islet cells. Dispersed islet cells from 3-week-old (*A* and *B*) and 10-week-old (*C* and *D*) mice were incubated with 10 μmol/l DCF in Krebs-Ringer buffer containing 2.8 mmol/l glucose for 45 min at 37°C. After washing with Krebs-Ringer buffer, cell fluorescence was measured at 480 nm excitation and 510 nm emission using an Olympus fluorescent BX51W1 microscope. *A–D*: Representative fluorescent (*upper panel*) and light (*lower panel*) images of the islet cells. *E* and *F*: The average fluorescence intensity was calculated by tracing around each cell and averaging the fluorescence across the entire field of view. (*n* = 4 with three mice per genotype in each experiment.) mtDNA quantity (*G* and *H*) was calculated as the ratio of COX to β-actin DNA levels. (*n* = 3 with 8–10 mice per genotype in each experiment.) Data are means ± SE. *$P < 0.05$; ***$P < 0.01$ compared with age-matched WT. (A high-quality digital representation of this figure is available in the online issue.)

Mitochondria couple cellular metabolism with Ca^{2+} homeostasis and signaling. Several studies have suggested a role for enhanced mitochondrial Ca^{2+} in modulating ATP levels and insulin secretion from cells (rev. in 32); however, this idea is somewhat controversial (30,41). In turn, mitochondrial Ca^{2+} uptake is highly dependent on the potential gradient of the inner mitochondrial membrane. MKR pre-diabetic and diabetic β-cells exhibited significantly attenuated mitochondrial Ca^{2+} uptake in response

to glucose, which could not be accounted for by reduced cytosolic Ca^{2+} uptake. It is difficult to distinguish whether the lower mitochondrial Ca^{2+} capacity has reduced the activity and hence expression of enzymes regulating the TCA cycle (such as IDH2 and OGDH) to further augment the mitochondrial respiratory defect or if the reduced Ca^{2+} uptake is a consequence of impaired hyperpolarization of $\Delta\Psi_m$ due to a reduced flow of substrate through the electron transport chain. Regardless, the data support the
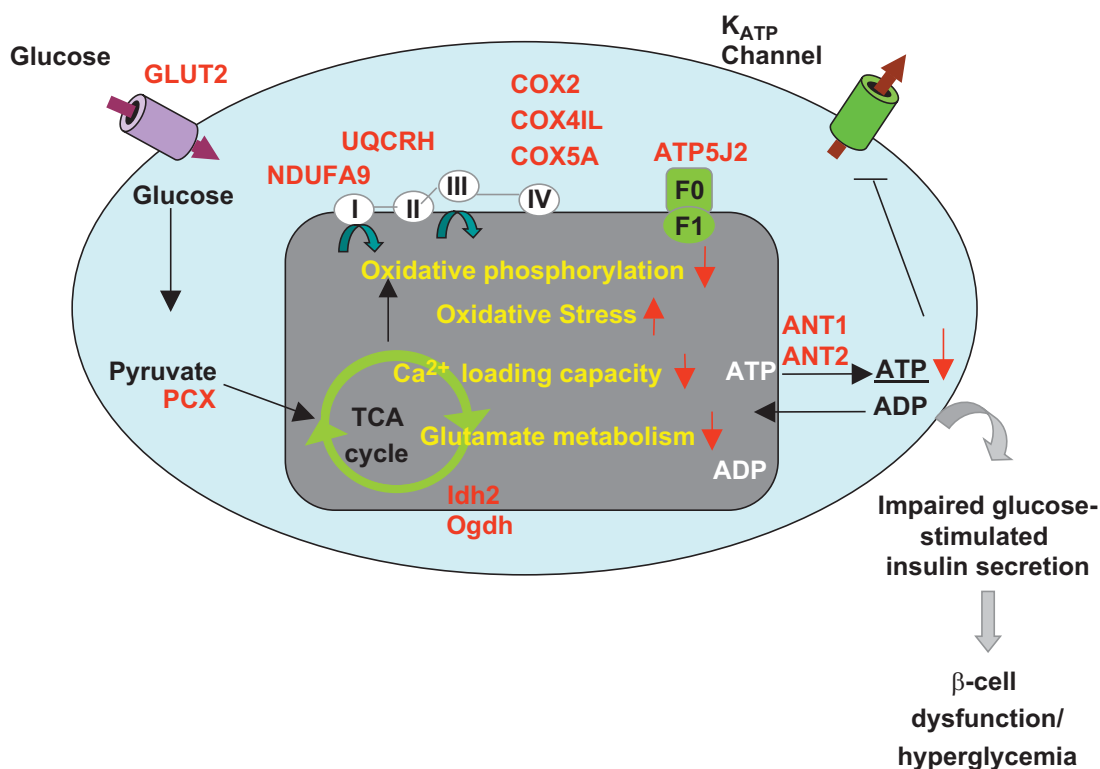
FIG. 7. Summary of the molecular and protein expression changes that lead to the dysfunctional metabolic phenotype in diabetic MKR islets. The proteins highlighted in red were significantly changed in MKR diabetic islets.

idea of reduced mitochondrial metabolic capacity in MKR islets just before and after the onset of hyperglycemia.

A potential consequence of mitochondrial dysfunction is increased production of ROS. Indeed, we observed that 10-week-old diabetic islets exhibited a twofold increase in the production of oxidized DCF but enhanced expression of antioxidant genes compared with control. Generally, increased ROS is a function both of the efficiency of transfer of electrons through the respiratory chain and the level of antioxidant defense in the cell (normally low in β-cells) (42). The enhanced antioxidant gene expression in diabetic MKR islets suggests a compensatory response for the increased oxidative stress (33). Therefore, it appears that the oxidative stress is probably a consequence not a cause of the mitochondrial metabolic dysfunction we observe in 10-week-old MKR islets. The proteomics study revealed decreased expression of a major mitochondrial antioxidant protein, manganese superoxide dismutase (SOD2), in MKR diabetic islet mitochondria. Interestingly, gene expression of Sod2 was not changed, again showing the importance of posttranslational modification. SOD2 converts superoxide to oxygen plus hydrogen peroxide and serves as the primary defense against mitochondrial superoxide accumulation (43). Impaired SOD2 activity has been found in islets from type 1 and 2 diabetic patients (44,45) and type 1 diabetic animals (46). Collectively, the increased oxidative stress and attenuated $\Delta\Psi_m$ in MKR islets potentially cause further deterioration of mitochondrial function.

The mitochondria of pre- and posthyperglycemic MKR β-cells were swollen and distorted with fewer dense core insulin granules. These data lend further support for the concept of altered mitochondrial function in the development of diabetes in MKR mice. The inner mitochondrial membrane protein, mitofilin (IMMT), which was recently reported to control cristae morphology and facilitate correct mitochondrial function (47), was decreased in MKR diabetic islets at the protein but not mRNA level (Fig. 5B), confirming again the importance of posttranslational modification in the regulation of the mitochondrial inner membrane. Downregulation of mitofilin in Hela cells caused a drastic change in the organization of the inner membrane and was associated with high ROS production (47). Thus, mitofilin may be a critical organizer of the mitochondrial cristae morphology and indispensable for normal mitochondrial function; however, this requires further validation. These changes in mitochondrial structure may be a biomarker for altered mitochondrial function. Several studies support that mitochondrial morphology and metabolism play a linked role in β-cell function and survival in vitro (9–11). In addition, hyperglycemia-induced ROS production caused dynamic changes in mitochondrial morphology (48), and hyperglycemia was associated with enlarged mitochondria in Zucker diabetic fatty (ZDF) rat islets (49). Exposure of human pancreatic islets to cytokines induced β-cell damage, caused mitochondrial swelling and enlargement, and ultimately reduced cell survival (50). A distorted morphology similar to that in MKR mouse islets has been reported in β-cell mitochondria from diabetic mice with impaired respiratory chain function (7) and human type 2 diabetic patients (12). Whether the decreased mitochondrial function seen in MKR diabetic islets was caused by reduced mitochondrial content or reduced functional capacity of mitochondria is unclear. Compared with control mice, we showed a significant decrease in mtDNA in MKR diabetic islets, which indicates that decreased mitochondrial content at least partly explains reduced mitochondrial metabolic coupling. However, when cytochrome c oxidase–dependent oxygen consumption rate was normalized to mtDNA,

a significant decrease was still observed. This result suggests that functional impairments in mitochondrial oxidative function are not fully accounted for by reduced mtDNA, but by the interplay of decreased mitochondrial function and content.

In conclusion, based on our analysis of the proteomic/ transcriptomic/metabolic phenotype of MKR mice, we propose the following sequence of events for the progression of insulin resistance to β-cell dysfunction (Fig. 7): the reduction of multiple proteins in the mitochondrial inner membrane impairs OxPhos, initiating a cycle of reduced redox-stimulated mitochondrial metabolic coupling factors, causing decreased $\Delta\Psi_m$ and mitochondrial Ca^{2+} capacity, a decline in ATP generation, and impaired GSIS. Concomitantly increased islet oxidative stress might further impair OxPhos and transduction of the glucose-sensing signal. Moreover, reduced expression of the adenine nucleotide translocator would inhibit the translocation of ATP to the cytosol, further inhibiting normal electron transport until the rate of ATP production falls below that of ATP demand, resulting in metabolic failure and impaired insulin secretion. Interestingly, many of the observed mitochondrial impairments and reduced GSIS occurred just before overt hyperglycemia and therefore suggest that improving mitochondrial function may improve defective β-cell secretion seen in type 2 diabetes.

ACKNOWLEDGMENTS

REFERENCES

1. Eriksson J, Franssila-Kallunki A, Ekstrand A, Saloranta C, Widen E, Schalin C, Groop L. Early metabolic defects in persons at increased risk for non-insulin-dependent diabetes mellitus. N Engl J Med 1989;321:337–343
2. Ferrannini E, Gastaldelli A, Miyazaki Y, Matsuda M, Pettiti M, Natali A, Mari A, DeFronzo RA. Predominant role of reduced beta-cell sensitivity to glucose over insulin resistance in impaired glucose tolerance. Diabetologia 2003;46:1211–1219
3. Weyer C, Bogardus C, Mott DM, Pratley RE. The natural history of insulin secretory dysfunction and insulin resistance in the pathogenesis of type 2 diabetes mellitus. J Clin Invest 1999;104:787–794
4. Matschinsky FM, Magnuson MA, Zelent D, Jetton TL, Doliba N, Han Y, Taub R, Grimsby J. The network of glucokinase-expressing cells in glucose homeostasis and the potential of glucokinase activators for diabetes therapy. Diabetes 2006;55:1–12
5. MacDonald MJ, Fahien LA. Insulin release in pancreatic islets by a glycolytic and a Krebs cycle intermediate: contrasting patterns of glyceraldehyde phosphate and succinate. Arch Biochem Biophys 1990;279:104–108
6. Dukes ID, McIntyre MS, Mertz RJ, Philipson LH, Roe MW, Spencer B, Worley JF 3rd. Dependence on NADH produced during glycolysis for beta-cell glucose signaling. J Biol Chem 1994;269:10979–10982
7. Silva JP, Kohler M, Graff C, Oldfors A, Magnuson MA, Berggren PO, Larsson NG. Impaired insulin secretion and beta-cell loss in tissue-specific knockout mice with mitochondrial diabetes. Nat Genet 2000;26:336–340
8. Maassen JA, 'T Hart LM, Van Essen E, Heine RJ, Nijpels G, Jahangir Tafrechi RS, Raap AK, Janssen GM, Lemkes HH. Mitochondrial diabetes: molecular mechanisms and clinical presentation. Diabetes 2004;53(Suppl. 1):S103–S109
9. Molina AJ, Wikstrom JD, Stiles L, Las G, Mohamed H, Elorza A, Walzer G, Twig G, Katz S, Corkey BE, Shirihai OS. Mitochondrial networking protects beta cells from nutrient induced apoptosis. Diabetes 2009;58:2303–2315
10. Park KS, Wiederkehr A, Kirkpatrick C, Mattenberger Y, Martinou JC, Marchetti P, Demaurex N, Wollheim CB. Selective actions of mitochondrial fission/fusion genes on metabolism-secretion coupling in insulin-releasing cells. J Biol Chem 2008;283:33347–33356
11. Twig G, Elorza A, Molina AJ, Mohamed H, Wikstrom JD, Walzer G, Stiles L, Haigh SE, Katz S, Las G, Alroy J, Wu M, Py BF, Yuan J, Deeney JT, Corkey BE, Shirihai OS. Fission and selective fusion govern mitochondrial segregation and elimination by autophagy. EMBO J 2008;27:433–446
12. Anello M, Lupi R, Spampinato D, Piro S, Masini M, Boggi U, Del Prato S, Rabuazzo AM, Purrello F, Marchetti P. Functional and morphological alterations of mitochondria in pancreatic beta cells from type 2 diabetic patients. Diabetologia 2005;48:282–289
13. Del Guerra S, Lupi R, Marselli L, Masini M, Bugliani M, Sbrana S, Torri S, Pollera M, Boggi U, Mosca F, Del Prato S, Marchetti P. Functional and molecular defects of pancreatic islets in human type 2 diabetes. Diabetes 2005;54:727–735
14. Mulder H, Ling C. Mitochondrial dysfunction in pancreatic beta-cells in type 2 diabetes. Mol Cell Endocrinol 2009;297:34–40
15. Petersen KF, Dufour S, Befroy D, Garcia R, Shulman GI. Impaired mitochondrial activity in the insulin-resistant offspring of patients with type 2 diabetes. N Engl J Med 2004;350:664–671
16. Bonnard C, Durand A, Peyrol S, Chanseaume E, Chauvin MA, Morio B, Vidal H, Rieusset J. Mitochondrial dysfunction results from oxidative stress in the skeletal muscle of diet-induced insulin-resistant mice. J Clin Invest 2008;118:789–800
17. Patti ME, Butte AJ, Crunkhorn S, Cusi K, Berria R, Kashyap S, Miyazaki Y, Kohane I, Costello M, Saccone R, Landaker EJ, Goldfine AB, Mun E, DeFronzo R, Finlayson J, Kahn CR, Mandarino LJ. Coordinated reduction of genes of oxidative metabolism in humans with insulin resistance and diabetes: potential role of PGC1 and NRF1. Proc Natl Acad Sci U S A 2003;100:8466–8471
18. Fernandez AM, Kim JK, Yakar S, Dupont J, Hernandez-Sanchez C, Castle AL, Filmore J, Shulman GI, Le Roith D. Functional inactivation of the IGF-I and insulin receptors in skeletal muscle causes type 2 diabetes. Genes Dev 2001;15:1926–1934
19. Asghar Z, Yau D, Chan F, Leroith D, Chan CB, Wheeler MB. Insulin resistance causes increased beta-cell mass but defective glucose-stimulated insulin secretion in a murine model of type 2 diabetes. Diabetologia 2006;49:90–99
20. Jacob S, Machann J, Rett K, Brechtel K, Volk A, Renn W, Maerker E, Matthaei S, Schick F, Claussen CD, Haring HU. Association of increased intramyocellular lipid content with insulin resistance in lean nondiabetic offspring of type 2 diabetic subjects. Diabetes 1999;48:1113–1119
21. Diao J, Allister EM, Koshkin V, Lee SC, Bhattacharjee A, Tang C, Giacca A, Chan CB, Wheeler MB. UCP2 is highly expressed in pancreatic alpha-cells and influences secretion and survival. Proc Natl Acad Sci U S A 2008;105:12057–12062
22. da Silva Xavier G, Loder MK, McDonald A, Tarasov AI, Carzaniga R, Kronenberger K, Barg S, Rutter GA. TCF7L2 regulates late events in insulin secretion from pancreatic islet beta-cells. Diabetes 2009;58:894–905
23. Goto M, Holgersson J, Kumagai-Braesch M, Korsgren O. The ADP/ATP ratio: a novel predictive assay for quality assessment of isolated pancreatic islets. Am J Transplant 2006;6:2483–2487
24. Lee S, Robson-Doucette C, Wheeler M. Uncoupling protein 2 regulates reactive oxygen species formation in islets and influences susceptibility to diabetogenic action of streptozotocin. J Endocrinol 2009;203:33–43
25. Di Paola M, Cocco T, Lorusso M. Ceramide interaction with the respiratory chain of heart mitochondria. Biochemistry 2000;39:6660–6668
26. Lu H, Yang Y, Allister EM, Wijesekara N, Wheeler MB. The identification of potential factors associated with the development of type 2 diabetes: a quantitative proteomics approach. Mol Cell Proteomics 2008;7:1434–1451
27. Zeeberg BR, Feng W, Wang G, Wang MD, Fojo AT, Sunshine M, Narasimhan S, Kane DW, Reinhold WC, Lababidi S, Bussey KJ, Riss J, Barrett JC, Weinstein JN. GoMiner: a resource for biological interpretation of genomic and proteomic data. Genome Biol 2003;4:R28
28. Dahlquist KD, Salomonis N, Vranizan K, Lawlor SC, Conklin BR. GenMAPP, a new tool for viewing and analyzing microarray data on biological pathways. Nat Genet 2002;31:19–20
29. Toyoshima Y, Gavrilova O, Yakar S, Jou W, Pack S, Asghar Z, Wheeler MB, LeRoith D. Leptin improves insulin resistance and hyperglycemia in a mouse model of type 2 diabetes. Endocrinology 2005;146:4024–4035
30. Heart E, Corkey RF, Wikstrom JD, Shirihai OS, Corkey BE. Glucose-dependent increase in mitochondrial membrane potential, but not cytoplasmic calcium, correlates with insulin secretion in single islet cells. Am J Physiol Endocrinol Metab 2006;290:E143–E148

31. Duchen MR, Smith PA, Ashcroft FM. Substrate-dependent changes in mitochondrial function, intracellular free calcium concentration and membrane channels in pancreatic beta-cells. Biochem J 1993;294:35–42

32. Wiederkehr A, Wollheim CB. Impact of mitochondrial calcium on the coupling of metabolism to insulin secretion in the pancreatic beta-cell. Cell Calcium 2008;44:64–76

33. Pi J, Bai Y, Daniel KW, Liu D, Lyght O, Edelstein D, Brownlee M, Corkey BE, Collins S. Persistent oxidative stress due to absence of uncoupling protein 2 associated with impaired pancreatic beta-cell function. Endocrinology 2009;150:3040–3048

34. Orrenius S. Reactive oxygen species in mitochondria-mediated cell death. Drug Metab Rev 2007;39:443–455

35. Zhao H, Yakar S, Gavrilova O, Sun H, Zhang Y, Kim H, Setser J, Jou W, LeRoith D. Phloridzin improves hyperglycemia but not hepatic insulin resistance in a transgenic mouse model of type 2 diabetes. Diabetes 2004;53:2901–2909

36. Napiwotzki J, Kadenbach B. Extramitochondrial ATP/ADP-ratios regulate cytochrome c oxidase activity via binding to the cytosolic domain of subunit IV. Biol Chem 1998;379:335–339

37. Kobayashi T, Nakanishi K, Nakase H, Kajio H, Okubo M, Murase T, Kosaka K. In situ characterization of islets in diabetes with a mitochondrial DNA mutation at nucleotide position 3243. Diabetes 1997;46:1567–1571

38. Maassen JA, Kadowaki T. Maternally inherited diabetes and deafness: a new diabetes subtype. Diabetologia 1996;39:375–382

39. Schiff M, Froissart R, Olsen RK, Acquaviva C, Vianey-Saban C. Electron transfer flavoprotein deficiency: functional and molecular aspects. Mol Genet Metab 2006;88:153–158

40. Yan LJ, Sohal RS. Mitochondrial adenine nucleotide translocase is modified oxidatively during aging. Proc Natl Acad Sci U S A 1998;95:12896–12901

41. Ravier MA, Eto K, Jonkers FC, Nenquin M, Kadowaki T, Henquin JC. The oscillatory behavior of pancreatic islets from mice with mitochondrial glycerol-3-phosphate dehydrogenase knockout. J Biol Chem 2000;275:1587–1593

42. Melov S. Mitochondrial oxidative stress: physiologic consequences and potential for a role in aging. Ann N Y Acad Sci 2000;908:219–225

43. Lebovitz RM, Zhang H, Vogel H, Cartwright J Jr, Dionne L, Lu N, Huang S, Matzuk MM. Neurodegeneration, myocardial injury, and perinatal death in mitochondrial superoxide dismutase-deficient mice. Proc Natl Acad Sci U S A 1996;93:9782–9787

44. Marchetti P, Del Guerra S, Marselli L, Lupi R, Masini M, Pollera M, Bugliani M, Boggi U, Vistoli F, Mosca F, Del Prato S. Pancreatic islets from type 2 diabetic patients have functional defects and increased apoptosis that are ameliorated by metformin. J Clin Endocrinol Metab 2004;89:5535–5541

45. Zotova EV, Chistiakov DA, Savost'ianov KV, Bursa TR, Galeev IV, Strokov IA, Nosikov VV. [Association of the SOD2 Ala(-9)Val and SOD3 Arg213Gly polymorphisms with diabetic polyneuropathy in patients with diabetes mellitus type 1]. Mol Biol (Mosk) 2003;37:404–408 [in Russian]

46. Weiss H, Bleich A, Hedrich HJ, Kolsch B, Elsner M, Jorns A, Lenzen S, Tiedge M, Wedekind D. Genetic analysis of the LEW. 1AR1-iddm rat: an animal model for spontaneous diabetes mellitus. Mamm Genome 2005;16:432–441

47. John GB, Shang Y, Li L, Renken C, Mannella CA, Selker JM, Rangell L, Bennett MJ, Zha J. The mitochondrial inner membrane protein mitofilin controls cristae morphology. Mol Biol Cell 2005;16:1543–1554

48. Yu T, Robotham JL, Yoon Y. Increased production of reactive oxygen species in hyperglycemic conditions requires dynamic change of mitochondrial morphology. Proc Natl Acad Sci U S A 2006;103:2653–2658

49. Higa M, Zhou YT, Ravazzola M, Baetens D, Orci L, Unger RH. Troglitazone prevents mitochondrial alterations, beta cell destruction, and diabetes in obese prediabetic rats. Proc Natl Acad Sci U S A 1999;96:11513–11518

50. Trincavelli ML, Marselli L, Falleni A, Gremigni V, Ragge E, Dotta F, Santangelo C, Marchetti P, Lucacchini A, Martini C. Upregulation of mitochondrial peripheral benzodiazepine receptor expression by cytokine-induced damage of human pancreatic islets. J Cell Biochem 2002;84:636–644